

A numerical scheme and validation of the asymptotic energy release rate formula for a 2D gel thin film debonding problem

M. Carme Calderer^{*1}, Duvan Henao^{†2}, Manuel A. Sánchez^{‡3},
Ronald A. Siegel^{§4}, and Sichen Song^{¶1,4}

¹School of Mathematics, University of Minnesota. Minneapolis,
MN 55455

²Instituto de Ciencias de la Ingeniería, Universidad de O'Higgins.
Rancagua, Chile.

³Instituto de Ingeniería Matemática y Computacional, Pontificia
Universidad Católica de Chile. Santiago, Chile.

⁴Department of Pharmaceutics, University of Minnesota.
Minneapolis, MN 55455

February 3, 2023

Abstract

This article presents a numerical scheme for the variational model formulated by Calderer, Garavito, Henao, Tapia & Lyu [J. Elast. 141:51–73, 2020] for the debonding of a hydrogel film from a rigid substrate upon exposure to solvent, in the bidimensional case of a film placed between two parallel walls. It builds upon the scheme introduced by Song, Siegel, Sánchez,

^{*}calde014@umn.edu

[†]Corresponding author: duvan.henao@uoh.cl

[‡]manuel.sanchez@ing.puc.cl

[§]siege017@umn.edu

[¶]song0357@umn.edu

Calderer & Henao [J. Elast. doi:10.1007/s10659-022-09911-6, 2022] for completely bonded gels, which fails to be robust in the case of gels that are already debonded. The new scheme is used to compute the energy release rate function, based on which predictions are offered for the threshold thickness below which the gel/substrate system is stable against debonding. This study, in turn, makes it possible to validate a theoretical estimate for the energy release rate obtained in the mentioned works, which is based on a thin-film asymptotic analysis and which, due to its explicit nature, is potentially valuable in medical device development. An existence theorem and rigorous justifications of some approximations made in our numerical scheme are also provided.

Keywords: Gels, Debonding, Thin film, Nonlinear elasticity, Flory-Huggins

Mathematics Subject Classification (2020): 35B40, MSC 35J57, 74B20, 74G65, 74R99.

1 Introduction

In [CGH⁺20, SSS⁺22] a model was proposed for the debonding of a thin hydrogel film from a rigid substrate when exposed to solvent, combining the classical work by Flory & Rehner [FRJ43, FRJ44, Flo53] with the variational description of fracture [Gri21, FM98, BFM08]. It consists in the minimization of

$$(\mathbf{u}, \Gamma) \mapsto \int_{\Omega} \frac{G}{2} |\mathbf{F}|^2 dx + \int_{\Omega'} \frac{k_B T}{V_m} (\phi_1 \ln \phi_1 + \chi \phi_1 \phi_2) dy + \sigma \cdot \text{Area}(\Gamma), \quad (1)$$

$$\text{subject to } \begin{cases} \mathbf{u}(\mathbf{x}) = \mathbf{0}, & \text{for all } \mathbf{x} \in \Sigma \setminus \Gamma, \\ \mathbf{x} + \mathbf{u}(\mathbf{x}) \notin \Sigma, & \text{for all } \mathbf{x} \in \text{Int } \Omega \end{cases} \quad (2)$$

where $\Omega \subset \mathbb{R}^3$ is the region occupied initially by the synthesized gel (which is bonded to the substrate) as soon as it is immersed in solvent; Σ is the initial gel/substrate interface (Fig. 1); $\Omega' \subset \mathbb{R}^3$ is the region occupied after the gel, bonded to the substrate, is immersed in solvent and it reaches its swelling equilibrium (Fig. 2); $\mathbf{u} : \Omega \rightarrow \mathbb{R}^3$ is the displacement field describing the swelling of the gel; $\Gamma \subset \Sigma$ is the portion of the interface where the gel detaches from the substrate as a result of swelling (Fig. 2); $\text{Int } \Omega$ denotes the set of interior points of Ω ; the deformation gradient $\mathbf{I} + \nabla \mathbf{u}(\mathbf{x})$ is denoted by \mathbf{F} ; the prefactor $G > 0$ is the shear modulus of the gel in synthesis; the second integral is the Flory-Huggins energy

of mixing [Flo41, Hug41], [Doi13, Eq. 2.62], [RC⁺03, p. 143]; ϕ_1 and ϕ_2 are the solvent and polymer volume fractions in the deformed (swollen) configuration; σ is the adhesion energy; k_B is Boltzmann's constant; T is the temperature; V_m is the volume of one molecule of solvent; and χ is the chemical Flory-Huggins interaction parameter.

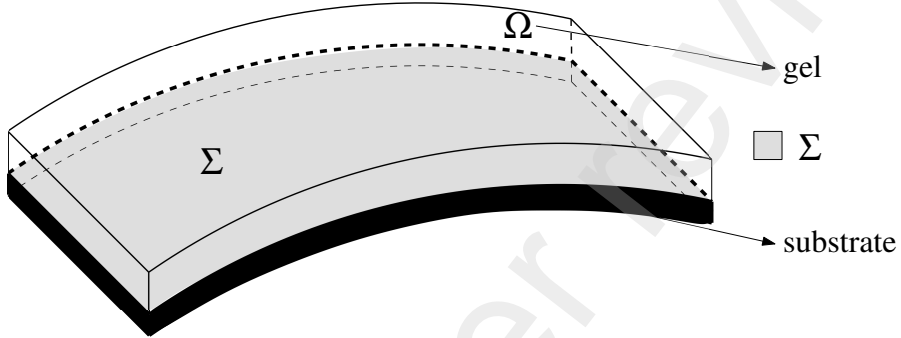


Figure 1: Reference configuration for a hydrogel/substrate system where the gel occupies the region Ω and it is initially bonded to the substrate below (across the curved interface Σ , colored in light grey).

The motivation comes from the design of the synthetic polymers that coat various medical implants, in order to estimate, for example, how thin the gel coating needs to be in order for it to be stable against debonding from the mechanical substrate. The model is being experimentally validated. One step in that direction was given in [SSS⁺22], where the case was considered of a rectangular Polyacrylamide (PAAm) gel,

$$\Omega = \{(x_1, x_2, x_3) : -\frac{\ell}{2} < x_1 < \frac{\ell}{2}, \quad 0 < x_2 < d, \quad -\frac{w}{2} < x_3 < \frac{w}{2}\}, \quad (3)$$

completely bonded ($\Gamma = \emptyset$) to a horizontal (x_1 - x_3 plane) glass substrate across the gel's bottom surface

$$\Sigma = \left(-\frac{\ell}{2}, \frac{\ell}{2}\right) \times \{0\} \times \left(-\frac{w}{2}, \frac{w}{2}\right) \quad (4)$$

(with x_2 representing the component in the vertical direction). Finite element simulations of the model, with parameters (shear modulus, initial polymer volume

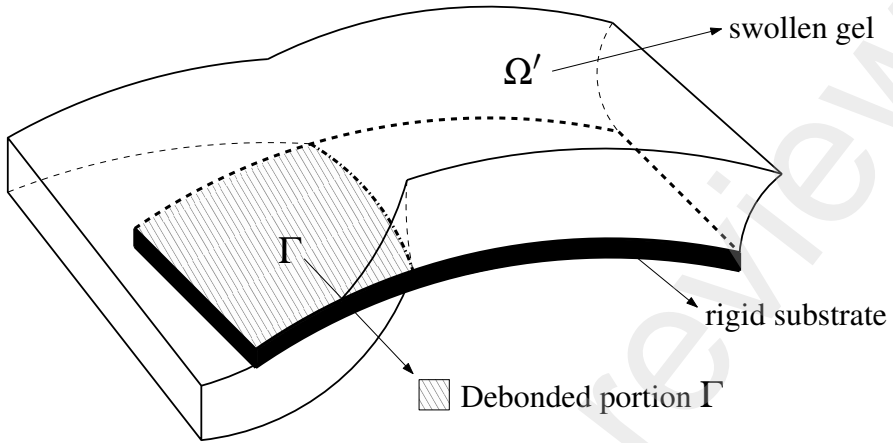


Figure 2: Schematic representation of the swelling of the gel after the gel/substrate system is immersed into solvent and the gel debonds on the portion Γ of the initial area of coverage Σ . (The lateral swelling at the debonded region is slightly amplified in the figure.)

fraction, and Flory-Huggins parameter) obtained from physical measurements, give an estimate of a stretch factor of 97% in the direction normal to the substrate, in good agreement with the 110% factor measured at the laboratory. Also, the numerical simulations captured the ‘bread-loafing’ effect with a lateral swelling of about 2 mm in all four lateral facets, the error relative to the experiments being of 4.3% along the width direction and of 6.7% along the length direction, for a sample with initial length, thickness, and width of 90 mm, 1.62 mm, and 15 mm.

This article proposes a numerical scheme for the model in a simplified 2D problem, on the two-dimensional domain

$$\Omega_2 = \{(x_1, x_2) : -\frac{\ell}{2} < x_1 < \frac{\ell}{2}, \quad 0 < x_2 < d\}, \quad (5)$$

and presents a numerical computation of the energy release rate function for various different geometries. In addition, with this numerical computation, a theoretical asymptotic estimation of the energy release rate, obtained in the idealized thin-film limit [CGH⁺20, Eqs. 84–85] [SSS⁺22, Eq. 67], is validated. Finally, rigorous proofs are provided to justify some approximations made in the numerical scheme.

1.1 Importance of the energy release rate function, explanation of the model, and formulation of the 2D simplification

If the bonds between the hydrogel and the substrate are broken on a portion Γ of the initial area of coverage Σ , the extra freedom attained by having the zero displacement constraint on a smaller part of the boundary $\partial\Omega$ allows the gel to reduce the Flory-Huggins part of the total energy (1). For most hydrogels this osmotic energy gain is larger than the additional cost due to elastic distortion, measured by the first term of the energy. If the total energy released were enough to compensate the fracture energy $\sigma \cdot \text{Area}(\Gamma)$ required for the breaking of those bonds, then the substrate/thin-gel-film system is expected to be unstable against debonding. Therefore, conditions are sought ensuring that (\mathbf{u}, Γ) , with $\Gamma = \emptyset$ (that is, no detachment), for some suitable displacement field \mathbf{u} , is a minimizer of the constrained variational problem (which is posed with the detachment region Γ , chosen among a suitable family of subsets of the whole initial interface Σ , as one of the unknowns). In particular, it is of interest to determine how thin the gel film needs to be in order for $\Gamma = \emptyset$ to be a minimizer.

The zero-displacement constraint in (2) on $\Sigma \setminus \Gamma$ models the bonding to the infinitely rigid substrate. On the other hand, the constraint $\mathbf{x} + \mathbf{u}(\mathbf{x}) \notin \Sigma$ for all points \mathbf{x} in the interior of Ω prevents the gel to interpenetrate the substrate.

The variational setting proposed in the functional (1) has the potential to shed light, in future studies, on the role played by the curvature of the substrate on the initiation of the debonding, as well as to capture curved and possibly irregular peeling fronts (corresponding to subsets Γ of the interface Σ with curved or even fractal boundaries, and having possibly many connected components). However, the scope of this article is restricted to the simplified hypothetical situation of a rectangular gel (see Eq. (3)) bonded to a flat substrate and placed between two parallel walls at the front and at the back (along the planes $x_3 = \frac{w}{2}$ and $x_3 = -\frac{w}{2}$, respectively), along which it is free to slide. Furthermore, the debonding will be assumed to be produced at the left and right ends of the interface with the substrate, and the detached portion Γ of the interface will be assumed to be symmetric with respect to the vertical plane $\{\mathbf{x} \in \mathbb{R}^3 : x_1 = 0\}$. Letting $\delta \in [0, 1]$ denote the *bonded fraction*, i.e. the fraction of Σ that remains bounded, the debonded region is then

$$\Gamma_\delta = \{(x_1, x_2, x_3) \in \Sigma : |x_1| \geq \frac{\delta w}{2}\},$$

(with Σ being that of Eq. (4)) and a minimizer of the hydrogel energy is sought

among maps of the form

$$\mathbf{u}(x_1, x_2, x_3) = \left(u(x_1, x_2), v(x_1, x_2), 0 \right), \quad \mathbf{x} = (x_1, x_2, x_3) \in \Omega.$$

The gel is assumed to be a saturated immiscible mixture with incompressible constituents, so that

$$\phi_1(\mathbf{y}(\mathbf{x})) = 1 - \phi(\mathbf{y}(\mathbf{x})) \quad \text{and} \quad \phi(\mathbf{y}(\mathbf{x})) \det \nabla \mathbf{y}(\mathbf{x}) = \phi_0 \quad \text{for all } \mathbf{x} \in \Omega,$$

where ϕ denotes the polymer volume fraction $\phi = \phi_2$ in the deformed configuration, $\phi_0 < 1$ is the initial polymer volume fraction in Ω (before exposure to solvent), and $\mathbf{y} : \Omega \rightarrow \mathbb{R}^3$ is the deformation map

$$\begin{aligned} \mathbf{y}(x_1, x_2, x_3) &= \left(y_1(x_1, x_2), y_2(x_1, x_2), x_3 \right), \quad (x_1, x_2, x_3) \in \Omega, \\ y_1(x_1, x_2) &:= x_1 + u(x_1, x_2), \quad y_2(x_1, x_2) := x_2 + v(x_1, x_2). \end{aligned} \tag{6}$$

In our experiments the PAAm gel film is chemically anchored in synthesis to a glass slide that is actually larger than the gel mold [SSS⁺22, Sect. 2.2.4], so the constraint (2b) becomes now

$$x_2 + v(x_1, x_2) \geq 0 \quad \text{for almost every } (x_1, x_2) \in \Omega_2. \tag{7}$$

The deformation gradient is

$$\mathbf{F}(\mathbf{x}) := \nabla \mathbf{y}(\mathbf{x}) = \begin{pmatrix} 1 + \partial_1 u & \partial_2 u & 0 \\ \partial_1 v & 1 + \partial_2 v & 0 \\ 0 & 0 & 1 \end{pmatrix}, \quad J := \det F = \frac{\partial(y_1, y_2)}{\partial(x_1, x_2)}.$$

Since it is independent of x_3 , it makes sense to study the energy per unit width. In the sequel all lengths will be taken to be in mm, and the shear modulus and the ratio $\frac{k_B T}{V_m}$ in MPa. Hence, we study the functional

$$\int_{\Omega_2} \frac{G}{2} |\mathbf{F}(\mathbf{x})|^2 + \frac{k_B T}{V_m} H(J(\mathbf{x})) dx_2 dx_1,$$

its value being interpreted as the energy, in mJ/mm, per unit millimeter of the width of the gel, with

$$H(J) := J \cdot (\phi_1 \ln \phi_1 + \chi \phi_1 \phi_2) = (J - \phi_0) \ln(1 - \phi) + \chi \phi_0(1 - \phi), \tag{8}$$

and $\phi = \phi_0/J$, corresponding to the entropy of mixing per unit reference volume.

In preparation for well-posedness (see Section 2), consider the space

$$\mathcal{A}_\delta := \left\{ (u, v) \in H^1(\Omega_2)^2 : J(\mathbf{x}) \geq \phi_0 \text{ almost everywhere, the corresponding deformation map } \mathbf{y} \text{ is one-to-one almost everywhere in } \Omega, \text{ and} \right.$$

deformation map \mathbf{y} is one-to-one almost everywhere in Ω , and

$$\left. u(x_1, 0) = v(x_1, 0) = 0 \quad \text{for all } |x_1| < \frac{\delta\ell}{2} \right\}. \quad (9)$$

Here H^1 is the standard Hilbert space of weakly differentiable square-integrable functions with square-integrable approximate gradients (see, e.g. [Eva10, EG92]); the constraint $\det \nabla \mathbf{y} > 0$ ensures the preservation of orientation; and the injectivity constraint (whose precise statement is that there exists a Lebesgue-zero measure set $N \subset \Omega$ such that the restriction $\mathbf{y}|_{\Omega \setminus N} : \Omega \setminus N \rightarrow \mathbb{R}^3$ is one-to-one, see [Bal81]) prevents the interpenetration of matter.

From now on, gravity will be taken into account, hence define

$$E[u, v] := \int_{\Omega_2} \left(\frac{G}{2} |\mathbf{F}(\mathbf{x})|^2 + \frac{k_B T}{V_m} H(J(\mathbf{x})) + \rho g v(x_1, x_2) - C \right) dx_2 dx_1, \quad (10)$$

where $g = 9.8$, ρ is the value in kg/mm³ of the density of the gel in the reference configuration, and

$$C := \min \left\{ \frac{G}{2} (3\lambda^2) + \frac{k_B T}{V_m} H(\lambda^3) : \lambda > 1 \right\}$$

so that $E[u, v]$ can be interpreted as the difference in energy (per unit width) compared to the isotropic expansion obtained (when furthermore gravity is neglected) in the unconstrained free swelling state. For each $0 \leq \delta \leq 1$ define:

$$\mathcal{E}_{\min}[\delta] := \min \left\{ E[u, v] : (u, v) \in \mathcal{A}_\delta \text{ such that (7) is satisfied} \right\}. \quad (11)$$

In the context delimited above, define the energy release rate function as

$$R[\delta] := \frac{\frac{d}{d\delta} \left(w \cdot \mathcal{E}_{\min}[\delta] \right)}{\frac{d}{d\delta} \text{Area}(\Gamma_\delta)} = \frac{1}{\ell} \frac{d\mathcal{E}_{\min}[\delta]}{d\delta}, \quad (12)$$

which measures the magnitude of the total energy released per unit increase in debonded area. From the energy minimization point of view of (1), a pre-existing ‘crack’ Γ_δ will grow if $R[\delta]$ is larger than or equal to the energy per unit area σ required to separate the gel from the substrate (steadily if $R[\delta]$ is exactly equal to σ and in an abrupt manner if $R[\delta] > \sigma$). In particular, the criterion for the completely bonded gel to be stable against debonding is $R[1] < \sigma$. This explains the importance of calculating this energy release rate function.

The asymptotic analyses in [CGH⁺20, Eqs. 84-85] [SSS⁺22, Eq. 67] [CH23] show that for thin films the minimizer (u_δ, v_δ) for the problem in (11) resembles the (displacement field corresponding to the) piecewise deformation

$$y_1(x_1, x_2) = \begin{cases} x_1, & |x_1| \leq \delta\ell/2, \\ \pm\delta\ell/2 + \lambda^*(x_1 - \delta\ell/2), & |x_1| \geq \delta\ell/2, \end{cases}$$

$$y_2(x_1, x_2) = \begin{cases} \lambda_{\text{uni}}x_2, & |x_1| \leq \delta\ell/2, \\ \lambda^*x_2, & |x_1| \geq \delta\ell/2, \end{cases}$$

with a transition layer around $|x_1| = \delta\ell/2$, of a size comparable to the gel’s thickness, where the equibiaxial and uniaxial stretch factors λ^* and λ_{uni} correspond, respectively, to the minimizers of $\frac{G}{2}|\mathbf{F}|^2 + \frac{k_B T}{V_m}H(\det \mathbf{F})$ among matrices of the form $\mathbf{F} = \text{diag}(\lambda, \lambda, 1)$ and among matrices of the form $\mathbf{F} = \text{diag}(1, \lambda, 1)$. They are determined implicitly by

$$\gamma + H'(\lambda^{*2}) = 0, \quad \gamma\lambda_{\text{uni}} + H'(\lambda_{\text{uni}}) = 0, \quad \gamma := \frac{G}{k_B T / V_m}. \quad (13)$$

This yields the approximation for the energy release rate function that

$$R[\delta] \approx d \left(\left(\frac{G}{2}(2 + \lambda_{\text{uni}}^2) + \frac{k_B T}{V_m}H(\lambda_{\text{uni}}) \right) \right. \\ \left. - \left(\frac{G}{2}(2(\lambda^{*2}) + 1) + \frac{k_B T}{V_m}H((\lambda^*)^2) \right) \right) + \rho g \frac{d^2}{2}(\lambda_{\text{uni}} - \lambda^*). \quad (14)$$

If gravity (which is about four orders of magnitude smaller than the osmotic-elastic energy $\iint \frac{G}{2}|\mathbf{F}|^2 + \frac{k_B T}{V_m}H(\det \mathbf{F}) - C$) is neglected, the formula becomes

$$R[\delta] \approx d \left(\left(\frac{G}{2}(2 + \lambda_{\text{uni}}^2) + \frac{k_B T}{V_m}H(\lambda_{\text{uni}}) \right) - \left(\frac{G}{2}(2(\lambda^{*2}) + 1) + \frac{k_B T}{V_m}H((\lambda^*)^2) \right) \right). \quad (15)$$

The above suggests that $R[\delta]$ is proportional to the gel's thickness d and is independent of δ , which translates into the criterion that the gel's thickness d should be less than the threshold value of

$$d_{\max} := \sigma / \left(\frac{G}{2}(2 + \lambda_{\text{uni}}^2) + \frac{k_B T}{V_m} H(\lambda_{\text{uni}}) - \frac{G}{2}(2(\lambda^*)^2 + 1) - \frac{k_B T}{V_m} H(\lambda^*) \right) \quad (16)$$

in order to prevent it from debonding. The explicit nature of this formula makes it potentially valuable in medical device development.

In this article (Section 5) we present a finite element analysis showing that the estimate (15) is indeed valid for a range of aspect ratios and a range of bonded fractions δ . Specifically, the constant value (15) predicted in the theoretical limit captures, up to a 5% relative error, the real value of the energy release rate for all $\delta \in (0.35, 0.89)$ when the thickness-to-length aspect ratio is of 5.6%; for $\delta \in (0.22, 0.94)$ when the aspect ratio is of 3.3%; and for $\delta \in (0.13, 0.97)$ when the aspect ratio is of 1.8%.

1.2 Outline of the article

In Section 2 we provide a rigorous proof of existence of solutions to the minimization problem (11) (for fixed bonded fraction δ ; comprising the gravitational, elastic, and mixing terms; and taking into account the obstacle constraint (7)). In Section 3 we rigorously justify, by Γ -convergence, the penalization approach of minimizing $E[u, v] + E_{A, \text{obstacle}}[u, v]$, with the penalty term $E_{A, \text{obstacle}}$ defined in (17), as a scheme for numerically implementing the obstacle constraint. In Section 4 we present a new numerical scheme for the gel debonding problem, showing its validity by comparison, using various metrics, against another numerical scheme that is known to be physically correct but which turns out not to be numerically robust. In Section 5 we present a finite element study showing the validity of the thin-film limit formula (15) for the energy release rate. Finally, in Section 6 we draw the conclusions of our work.

2 Existence of minimizers

As mentioned in [CGH⁺20, p. 56] [SSS⁺22, Sect. 3.1], when the Flory-Huggins parameter χ lies between 0 and $\frac{1}{2}$ the function $H(J)$ in (8) is convex. Hence, in this mixing regime the integrand $\frac{G}{2}|\mathbf{F}|^2 + \frac{k_B T}{V_m} H(\det \mathbf{F})$ falls in the class of poly-convex functions [Bal77, Cia88, Dac08a] (namely, convex functions of the vector

containing all the minors of \mathbf{F} as well as all of its components) in which it has been possible to prove the existence of minimizers (see, e.g., [Cia88, Dac08a, GMS89, Mül88, MÖ90, MTY94]), beginning with the pioneering work of Ball [Bal77]. Obtaining an existence theorem in the full 3D setting, with the quadratic neoHookean energy for the elastic distortion (instead of the more tractable variants where the growth of the stored-energy function is controlled from below by a power $C|\mathbf{F}|^p$ with an exponent $p > 2$) remains an open problem [CDL03, Muc10, HR18, BHMC23a, BHMC23b, DHM23]. In contrast, for the simplified 2D problem under consideration, in which the coercivity exponent equals the space dimension, the result by Müller [MÖ90] for the pure polymer model can be adapted to the case of a mixture with a fluid constituent, as is shown below.

Theorem 1. *For every bonded fraction $\delta \in [0, 1]$, $\phi_0 \in (0, 1)$, $\chi \in (0, \frac{1}{2})$, there exists a minimizer for the variational problem (11).*

Proof. The proof will be obtained using the direct method of the calculus of variations (see, e.g., [Cia88, Dac08a, Dac08b]). Recall first [Doi13, Sect. 2.4] [SSS⁺22, Eqs. 15 and 18] that

$$\begin{aligned} H'(J) &= \ln(1 - \phi) + \phi + \chi\phi^2, \\ H''(J) &= \frac{\phi}{J} \left(\frac{1}{1 - \phi} - 1 - 2\chi\phi \right), \quad \phi = \frac{\phi_0}{J}. \end{aligned}$$

One particular consequence is that $H(J)$ is decreasing since $\lim H(J) = 0$ as $J \rightarrow \infty$ and $H'(J)$ is increasing. Therefore, $H(J) \geq -\phi_0(1 - \chi)$ for all J , because that is its limit value when $J \rightarrow \infty$. This, combined with the obstacle inequality (7) and that $-x_2 \geq -d$, yields that the functional $E[u, v]$ in (10) is bounded from below in the class of maps considered in (11), namely, maps (u, v) in \mathcal{A}_δ satisfying (7).

Consider a minimizing sequence $(u^{(j)}, v^{(j)})$, for $j \in \mathbb{N}$, for the problem (11). For each $j \in \mathbb{N}$ let $\mathbf{y}^{(j)}$ be the corresponding deformation map, defined in (6). Since $\int |\nabla \mathbf{y}^{(j)}|^2$ is bounded above, by Poincaré's inequality (using the zero displacement boundary condition in the definition (9) of \mathcal{A}_δ) it follows that $(u^{(j)}, v^{(j)})$, for $j \in \mathbb{N}$, is bounded in H^1 and that it is possible to extract a subsequence (not relabelled) converging weakly in H^1 to some limit displacement field

$$(u_0, v_0) \in H^1(\Omega_2)^2.$$

Furthermore, by the continuity of the trace operator,

$$u_0(x_1, 0) = v_0(x_1, 0) = 0 \quad \text{for all } |x_1| < \frac{\delta\ell}{2}.$$

Since (passing to a subsequence) $v^{(j)}(x_1, x_2) \rightarrow v(x_1, x_2)$ pointwise a.e., the limit map v_0 satisfies the obstacle constraint (7). The next step consists in showing that (u_0, v_0) belongs to \mathcal{A}_δ .

The higher integrability of the Jacobian determinant due to Müller [M90], which holds in our problem because the exponent of integrability for the deformation gradients coincides with the space dimension in the simplified problem of the gel confined between parallel walls, gives the equiintegrability for the sequence $(\det \nabla \mathbf{y}^{(j)})$, for $j \in \mathbb{N}$. Since also $\text{Det } \nabla \mathbf{y}^{(j)} = \det \nabla \mathbf{y}^{(j)}$ for all j and

$$\text{Det } \nabla \mathbf{y}^{(j)} \rightarrow \text{Det } \nabla \mathbf{y}_0 \quad \text{in the distributional sense}$$

(see [Bal77]), where $\text{Det } \nabla \mathbf{y}^{(j)}$ is the distributional determinant and \mathbf{y}_0 is the deformation map associated to the displacement field (u_0, v_0) , it follows that $\det \nabla \mathbf{y}^{(j)}$ converges weakly in L^1 to $\det \nabla \mathbf{y}_0$. Consequently, by Mazur's theorem, $\det \nabla \mathbf{y}_0 \geq \phi_0$ since $\{f \in L^1(\Omega) : f(\mathbf{x}) \geq \phi_0 \text{ for a.e. } \mathbf{x} \in \Omega\}$ is convex and closed in L^1 .

Regarding the a.e. injectivity of the weak limit, the first results are due to Ball [Bal81] and Ciarlet & Nečas [CN87], who consider the case when the integrability is above the space dimension and use the embedding into the space of Hölder functions and the uniform convergence for weak limits (see also [Šve88, MS95]). For the quadratic energy at hand, the passage to the weak limit of the a.e. injectivity condition is a consequence of [HMC10], since the constraint $\det \nabla \mathbf{y} \geq \phi_0$ guarantees, in particular, that the Jacobian is positive a.e.

The above establishes the weak compactness of the subclass of \mathcal{A}_δ where (7) and an a priori energy upper bound is satisfied. The existence theorem now follows by using the lower semicontinuity theorem of [BCO81, Thm. 5.4], given the weak convergence of $\nabla \mathbf{y}^{(j)}$ in $L^2(\Omega, \mathbb{R}^{3 \times 3})$, the weak convergence in L^1 of $\det \nabla \mathbf{y}^{(j)}$, and the convexity of $H(J)$. □

3 Penalization approach for the obstacle problem

In our numerical computations the obstacle problem (7) is approximated by adding the penalty term

$$E_{\text{obstacle}, A}[u, v] := A \int_{\Omega_2} |(x_2 + v(x_1, x_2))^-|^2 dx_2 dx_1, \quad (17)$$

where the expression $(s)^- := \max\{0, -s\}$ above denotes the negative part of s . For the physically measured choice of parameters $G = 0.13 \text{ MPa}$, $\rho = 1.23E-6 \text{ kg mm}^{-3}$,

$\phi_0 = 0.2$, $\chi = 0.348$, the simulations were made with the value $A = 10^5$. In this section that penalization approach is justified using Γ -convergence [Dal93, Bra02], that is, by proving that as $A \rightarrow \infty$ minimizers of the problem with $E_{\text{obstacle},A}$ converge to a minimizer of the original variational problem with the obstacle constraint (7).

Note that for each $A > 0$ and $\delta \in [0, 1]$ fixed, essentially the same proof of Theorem 1 shows the existence of a minimizer of $E + E_{\text{obstacle},A}$ in the class \mathcal{A}_δ . The main difference is that a new argument is required in order to obtain that the energy (per unit width of gel) is bounded from below. One alternative is to observe that the gravitational energy (per unit width) is absorbed by the quadratic penalty term:

$$\rho g v(x_1, x_2) \geq \rho g \min\{-2\rho g/A - d, v(x_1, x_2)\}.$$

In those points where $v(x_1, x_2) \leq -2\rho g/A - d$, the following holds:

$$x_2 + v \leq d + v \leq -2\rho g/A$$

$$\rho g v = \rho g(x_2 + v - x_2) = -\rho g|(x_2 + v)^-| - \rho g x_2 \geq -\rho g \frac{|(x_2 + v)^-|^2}{2\rho g/A} - \rho g d.$$

Thus, for every $(x_1, x_2) \in \Omega_2$,

$$\rho g v(x_1, x_2) \geq \left(-2(\rho g)^2/A - \rho g d\right) - \frac{A}{2}|(x_2 + v)^-|^2 - \rho g d.$$

Consequently,

$$\begin{aligned} & \int_{\Omega_2} \rho g v(x_1, x_2) + A|(x_2 + v)^-|^2 dx_2 dx_1 \\ & \geq \frac{A}{2} \underbrace{\int_{\Omega_2} |(x_2 + v)^-|^2 dx_2 dx_1}_{\geq 0} - 2(\rho g)^2 \ell d/A - 2\rho g \ell d^2, \end{aligned} \quad (18)$$

which gives that the new energy is bounded from below, as wanted.

Theorem 2. Fix the bonded fraction $\delta \in [0, 1]$, $\phi_0 \in (0, 1)$, and $\chi \in (0, \frac{1}{2})$. Let $(A^{(j)})$ be an unbounded increasing sequence of positive numbers. Suppose that for each $j \in \mathbb{N}$ the pair $(u^{(j)}, v^{(j)})$ minimizes the functional $E + E_{\text{obstacle},A^{(j)}}$ in the class \mathcal{A}_δ . Then there exists a subsequence that converges weakly in H^1 to a solution of (11).

Proof. Note that the identity map $u \equiv 0$, $v \equiv 0$, $\mathbf{y}(\mathbf{x}) \equiv x$, $J \equiv 1$ belongs to the admissible class \mathcal{A}_δ . Since for all $j \in \mathbb{N}$

$$E_{\text{obstacle}, A^{(j)}}[0, 0] = A^{(j)} \int_{\Omega_2} |(x_2 + 0)^-|^2 dx_2 dx_1 = 0,$$

the total energy of the identity map is

$$\begin{aligned} E_0 &= E[0, 0] + E_{\text{obstacle}, A^{(j)}}[0, 0] \\ &= \ell \cdot d \cdot \left(\frac{3}{2}G + \frac{k_B T}{V_m} ((1 - \phi_0) \ln(1 - \phi_0) + \chi \phi_0 (1 - \phi_0)) - C \right). \end{aligned}$$

For each $j \in \mathbb{N}$

$$E[u^{(j)}, v^{(j)}] + E_{\text{obstacle}, A^{(j)}}[u^{(j)}, v^{(j)}] \leq E[0, 0] + E_{\text{obstacle}, A^{(j)}}[0, 0] = E_0,$$

because $(u^{(j)}, v^{(j)})$ is a minimizer. On the other hand, using (18) and the lower bound for $H(J)$ in the proof of Theorem 1,

$$\begin{aligned} E[u^{(j)}, v^{(j)}] + E_{\text{obstacle}, A^{(j)}} &\geq \frac{G}{2} \int |\nabla \mathbf{y}^{(j)}|^2 - (\phi_0(1 - \chi) + C)\ell d \\ &\quad + \frac{A^{(j)}}{2} \int \int |(x_2 + v^{(j)})^-|^2 - 2\rho g \ell d (\rho g / A^{(j)} + d). \end{aligned}$$

Thus, the L^2 -norm of the gradients $\nabla \mathbf{y}^{(j)}$ is bounded from above and

$$\int |(x_2 + v^{(j)})^-|^2 \leq \frac{2}{A^{(j)}} \left(E_0 + \ell d (\phi_0(1 - \chi) + C + 2(\rho g)^2 / A^{(j)} + 2\rho g d) \right).$$

As in Theorem 1, Poincaré's inequality together with the zero-displacement boundary condition yield the existence of a subsequence converging pointwise a. e., strongly in L^2 and weakly in H^1 to some limit map (u, v) .

That the limit deformation map is one-to-one a.e.; the zero-displacement boundary condition on $\Sigma \setminus \Gamma_\delta$; the bound $\det \nabla \mathbf{y}(\mathbf{x}) \geq \phi_0(\mathbf{x})$; and the weak L^1 convergence of the Jacobians are obtained as in Theorem 1. The convexity of $s \mapsto |(s)^-|^2$ yields the lower semicontinuity in

$$\int_{\Omega_2} |(x_2 + v(x_1, x_2))^-|^2 dx_2 dx_1 \leq \liminf_{j \rightarrow \infty} \int_{\Omega_2} |(x_2 + v^{(j)}(x_1, x_2))^-|^2 dx_2 dx_1 = 0,$$

hence the limit map satisfies the obstacle constraint (7).

It remains to prove that (u, v) minimizes the energy E among all maps in \mathcal{A}_δ satisfying the obstacle constraint. Let (\tilde{u}, \tilde{v}) be any such map. Since $x_2 + v(x_1, x_2) \geq 0$ for a.e. (x_1, x_2) ,

$$E[\tilde{u}, \tilde{v}] = E[\tilde{u}, \tilde{v}] + E_{\text{obstacle}, A^{(j)}}[\tilde{u}, \tilde{v}] \geq E[\tilde{u}^{(j)}, \tilde{v}^{(j)}] + E_{\text{obstacle}, A^{(j)}}[\tilde{u}^{(j)}, \tilde{v}^{(j)}]$$

By virtue of the strong L^2 convergence, the weak L^1 convergence of the Jacobians, and the convexity of $H(J)$, it is possible to invoke the lower semicontinuity theorem in [BCO81, Thm. 5.4] and conclude that

$$E[\tilde{u}, \tilde{v}] \geq E[u, v] \quad \text{for all } (\tilde{u}, \tilde{v}) \in \mathcal{A}_\delta \text{ satisfying (7).}$$

This finishes the proof. □

4 Numerical scheme for the 2D simulations

In this section we present a new numerical scheme for the gel debonding problem, where we replace the finite element space used in [SSS⁺22], conceived for the case of a completely bonded gel, with a finite element space in which an additional free-slip/zero-vertical-displacement boundary condition is implemented. It has the advantage of being significantly more robust, allowing the approximation to converge for almost the entire range of fractions $\delta \in (0, 1)$ of bonded interface, in contrast with the method in [SSS⁺22] (which here adopts the form of a traction-free boundary condition on the debonded part of the interface) where the code breaks down except for a small window of values of δ . We prove also that adopting the new numerical scheme comes at essentially no cost in terms of numerical errors.

The numerical scheme consists of:

- The penalization approach of Section 3 for the obstacle constraint.
- A third-order finite element discretization of the total energy functional.
- A novel free-slip/zero-vertical-displacement boundary condition on the debonded portion of the interface, together with a zero-displacement boundary condition on the bonded part of the interface.

- The incremental softening technique introduced in [SSS⁺²²] for the gel problem, in order to handle degeneracies of the Newton's method when the tangent stiffness is computed at states of large deformation.

The discrete nonlinear system obtained from the third-order finite element variational formulation of the minimization problem (which includes the penalization approach of Section 3 for the obstacle constraint (7)) is derived in Section 4.2. A complete explanation of the incremental softening technique for the study of gels, which in [SSS⁺²², Sect. 4.1] is only briefly described, is provided here in Section 4.3. The ranges of δ for which the traction-free problem collapses, as well as the ranges of δ for which our new numerical scheme succeeds, are detailed in Section 4.4. The validation of the numerical scheme, with a precise account of the various metrics in which the results were compared against the solutions of the traction-free scheme (for those values of δ where that scheme was able to converge), is also presented in Section 4.4.

4.1 Parameters and system of units

Recall (page 6) that in the energy functional $E[u, v]$ of (10) all lengths are taken to be in mm; the shear modulus G and the ratio $\frac{k_B T}{V_m}$ in MPa; the density ρ in the reference configuration in kg mm^{-3} ; and the gravitational acceleration g in m s^{-2} . In Table 1, we report the parameters used in our computations, based on the measurements in [SSS⁺²², Sects. 2 and 3.4].

Table 1: Parameters used in the computational model.

G [MPa]	$k_B T / V_m$ [MPa]	ϕ_0	χ	ρ [kg mm^{-3}]	g [m s^{-2}]
1.3E-1	1.366E+2	2.0E-1	3.48E-1	1.23E-6	9.8

Also, the values of the functional are to be interpreted as energy difference, in mJ mm^{-1} , per unit millimeter of width of the gel, with respect to the energy per unit millimeter of width of the isotropic expansion obtained in free swelling without gravity. Simulations seek for a minimizer of $E[u, v] + E_{\text{obstacle}, A}[u, v]$, in the appropriate admissible space, with $A = 10^5$.

In this study, we consider four different geometries, each with a length of $\ell = 90.00 \text{ mm}$ but with different thicknesses: $d = 1.62 \text{ mm}$, $d = 3.00 \text{ mm}$, $d = 5.00 \text{ mm}$, and $d = 15.00 \text{ mm}$, respectively.

4.2 Weak form of the equilibrium equations

Fix the bonded fraction $\delta \in (0, 1)$. Define

$$\widehat{\mathcal{A}}_\delta := \left\{ (\hat{u}, \hat{v}) \in H^1(\Omega_2)^2 : \hat{u}(x_1, 0) = \hat{v}(x_1, 0) = 0, \text{ for all } |x_1| < \frac{\delta\ell}{2} \right\}. \quad (19)$$

Formally, supposing that the constraint $J(\mathbf{x}) \geq \phi_0$ is always inactive (since we are studying the swelling and not the drying of the gels) and that considering only perturbations (\hat{u}, \hat{v}) that preserve the a.e. injectivity is sufficient to derive the variational form of the equations for test functions in the whole of the following function space, the Gâteaux derivative of the total energy (comprising both (10) and the obstacle penalization term $E_{\text{obstacle}, A}$) at $(u, v) \in \mathcal{A}_\delta$ in the direction $(\hat{u}, \hat{v}) \in \widehat{\mathcal{A}}_\delta$ is given by

$$\begin{aligned} a(u, v; \hat{u}, \hat{v}) := & \int_{\Omega_2} G((1 + \partial_1 u)\partial_1 \hat{u} + \partial_2 u \partial_2 \hat{u} + \partial_1 v \partial_1 \hat{v} + (1 + \partial_2 v)\partial_2 \hat{v}) \\ & + \frac{k_B T}{V_m} H'(J) \begin{pmatrix} 1 + \partial_2 v & -\partial_1 v \\ -\partial_2 u & 1 + \partial_1 u \end{pmatrix} \cdot \begin{pmatrix} \partial_1 \hat{u} & \partial_2 \hat{u} \\ \partial_1 \hat{v} & \partial_2 \hat{v} \end{pmatrix} + \rho g \hat{v} + 2A(x_2 + v)^- \hat{v} \, dx_2 \, dx_1. \end{aligned}$$

The weak form of the Euler-Lagrange equations

$$a(u, v; \hat{u}, \hat{v}) = 0 \quad \text{for all } \hat{u}, \hat{v} \text{ in } \mathcal{A}_\delta$$

delivers, as a consequence, the natural traction-free boundary condition on the debonded portion Γ of the interface Σ .

For the description of the finite element discretization, we base in part in [HH14, HMCX16]. We triangulate the domain using a regular triangular mesh \mathcal{T}_h (in the sense of Ciarlet [Cia78]), imposing a maximum value of $h = 0.4 \text{ mm}$ for the diameter of all elements in the triangulation and taking care that the bonded portion of the interface, $\{(x_1, 0) : x_1 \in (-\frac{\delta\ell}{2}, \frac{\delta\ell}{2})\}$, can be written as the union of the bottom segments of a certain number of elements (that is, both $(-\frac{\delta\ell}{2}, 0)$ and $(\frac{\delta\ell}{2}, 0)$ are the extreme vertex of some elements). We work with the third-order finite element space

$$X_h := \left\{ f \in C(\Omega_2) : (f|_T \in \mathcal{P}^3(T), \forall T \in \mathcal{T}_h) \wedge (f(x_1, 0) = 0, \text{ for all } |x_1| < \frac{\delta\ell}{2}) \right\}.$$

The finite element space for the displacement field is given by $(X_h)^2$. Since the boundary condition is zero on that portion of the interface, $(X_h)^2$ is also the finite element space for the variations (\hat{u}, \hat{v}) . For the variational problem

$$\text{minimize the total energy } E[u, v] + E_{\text{obstacle}, A}[u, v] \quad \text{in } (X_h)^2, \quad (20)$$

we arrive at the first order condition

$$a(u^h, v^h; \hat{u}^h, \hat{v}^h) = 0 \quad \text{for all } (\hat{u}^h, \hat{v}^h) \text{ in } (X_h)^2. \quad (21)$$

The basis (N_1, N_2, \dots, N_m) of X_h , is constructed based upon the triangulation \mathcal{T}_h . Thus, any $(u^h, v^h) \in (X_h)^2$ can be uniquely expanded as

$$u^h = \sum_{k=1}^m N_k u_k, \quad v^h = \sum_{k=1}^m N_k v_k, \quad (22)$$

where u_k and v_k are coefficients, real numbers, and $k \in \{1, \dots, m\}$, the number of degrees of freedom being $2m$. The energy can be rewritten as

$$\begin{aligned} E^h[\mathbf{v}] &= \int_{\Omega_2} \frac{G}{2} \left(2 + 2 \sum_{k=1}^m ((\partial_1 N_k) u_k + (\partial_2 N_k) v_k) + \sum_{j,k=1}^m \nabla N_j \cdot \nabla N_k (u_j u_k + v_j v_k) \right) \\ &\quad + \frac{k_B T}{V_m} H \left(1 + \sum_{k=1}^m ((\partial_1 N_k) u_k + (\partial_2 N_k) v_k) + \sum_{j,k=1}^m \det(\nabla N_j, \nabla N_k) u_j v_k \right) \\ &\quad + \sum_{k=1}^m \rho g N_k v_k - C + A |(x_2 + \sum_{k=1}^m N_k v_k)^{-}|^2 \end{aligned}$$

where $\mathbf{v} = (u_1, u_2, \dots, u_m, v_1, v_2, \dots, v_m)$. Since a is linear on \hat{u} and on \hat{v} , the weak discretized Euler-Lagrange equations (21) are equivalent to

$$a(u^h, v^h; N_k, 0) = 0 \quad \text{and} \quad a(u^h, v^h; 0, N_k) = 0 \quad \text{for all } k \in \{1, \dots, m\}. \quad (23)$$

This, in turn, is equivalent to the optimality condition $\mathbf{F}^h[\mathbf{v}] = \mathbf{0}$, with $\mathbf{F}^h[\mathbf{v}] = \nabla E^h[\mathbf{v}]$; and, more explicitly, to the following system of $2m$ nonlinear equations with $2m$ unknowns:

$$\begin{aligned} 0 = F_k^h[\mathbf{v}] &:= b_k + \sum_{j=1}^m a_{jk} u_j + \int_{\Omega_2} \frac{k_B T}{V_m} H' \left(1 + \sum_{k=1}^m ((\partial_1 N_k) u_k + (\partial_2 N_k) v_k) \right. \\ &\quad \left. + \sum_{j,k=1}^m \det(\nabla N_j, \nabla N_k) u_j v_k \right) \left(\partial_1 N_k + \sum_{\ell=1}^m \det(\nabla N_k, \nabla N_\ell) v_\ell \right) \end{aligned} \quad (24)$$

and

$$\begin{aligned} 0 = F_{m+k}^h[\mathbf{v}] &:= c_k + \sum_{j=1}^m a_{jk} v_j + \int_{\Omega_2} \frac{k_B T}{V_m} H' \left(1 + \sum_{k=1}^m ((\partial_1 N_k) u_k + (\partial_2 N_k) v_k) \right. \\ &\quad \left. + \sum_{j,k=1}^m \det(\nabla N_j, \nabla N_k) u_j v_k \right) \left(\partial_2 N_k + \sum_{j=1}^m \det(\nabla N_j, \nabla N_k) u_j \right) \\ &\quad + 2A \left(x_2 + \sum_{j=1}^m N_j v_j \right)^{-} N_k \end{aligned} \quad (25)$$

for all $k \in \{1, \dots, m\}$, where

$$\begin{aligned} b_k &:= \int_{\Omega_2} G \partial_1 N_k(x_1, x_2) dx_2 dx_1, \\ c_k &:= \int_{\Omega_2} G \partial_2 N_k(x_1, x_2) + \rho g N_k dx_2 dx_1, \\ a_{jk} &:= \int_{\Omega_2} G \nabla N_j \cdot \nabla N_k dx_2 dx_1. \end{aligned}$$

4.3 Incremental softening

The system of nonlinear equations arising from the finite element approximation of our nonlinear boundary value problems was solved using the damped Newton's method, with a damping parameter of $\alpha = 0.05$. However, the implementation of the Newton's method did not work well when the tangent stiffness was computed at states of large deformation. We implement the incremental softening technique proposed in [SSS⁺22], whereby the nonlinear system is solved first for gels that are much more rigid (for values of G about seven times larger than the desired 0.13 MPa) and then using the previous solution as the first iteration of the Newton's method for the next (smaller) value of G . In total, 16 different values of G were considered. Instead of working with a linearly spaced sequence of shear moduli G , we guided ourselves by the uniaxial stretch λ_{uni} of the thin-film limit solution (13), as an a priori estimate of the magnitude of the expected swelling. The first shear modulus considered (G_0) is the one of a gel rigid enough so that the predicted vertical stretch $\lambda_0 = \lambda_{\text{uni}}(G_0, \chi, \phi_0, T, V_m)$ at the middle of the gel is of only 10%:

$$\lambda_0 = 1.1, \quad G_0 \lambda_0 + \frac{k_B T}{V_m} H'(\lambda_0) = 0.$$

When $\chi = 0.348$, $\phi_0 = 0.2$, $T = 296\text{K}$, and $V_m = 2.992 \times 10^{-29} \text{m}^3$, the above gives $G_0 \approx 0.91 \text{MPa}$. The last shear modulus considered was G , corresponding to a theoretical stretch λ_{15} obtained implicitly from

$$G_{15} := G, \quad G \lambda_{15} + \frac{k_B T}{V_m} H'(\lambda_{15}) = 0.$$

For the parameters used in this article, $\lambda_{15} \approx 1.99$. The remaining shear moduli are, hence, defined as follows:

$$\lambda_i := \frac{(15-i)\lambda_0 + i\lambda_{15}}{15}, \quad G_i := -\frac{k_B T}{V_m} \frac{H'(\lambda_i)}{\lambda_i}, \quad i \in \{0, 1, \dots, 14\}.$$

In each of the 16 resolutions of the Newton's method, the stopping criteria used were defined to be that the absolute value of the inner product between the (vector of coefficients representing the) residuals and the difference of the successive solutions had to be less than a certain tolerance (or that a certain prescribed maximum number `maxits` of iterations were reached). The tolerance chosen for the stopping criteria was always 10^{-3} and `maxits=100`, except in the final resolution of the Newton's method, with the right value of G , where the tolerance for the stopping criteria was 10^{-6} and `maxits` was 500.

All in all, we work with the following algorithm.

Algorithm 1 Incremental softening

```

1: tol $\leftarrow 10^{-3}$ ; maxits $\leftarrow 100$ ;  $\alpha \leftarrow 0.05$ 
2:  $v \leftarrow 0$ 
3: for  $i$  from 0 to 15 do
4:   if  $i = 15$  then
5:     tol $\leftarrow 10^{-6}$ ; maxits $\leftarrow 500$ ;
6:   end if
7:    $G_{\text{parameter}} \leftarrow G_i$ 
8:   it $\leftarrow 0$ 
9:   while it < maxits do
10:    res $\leftarrow \mathbf{F}^h[G_{\text{parameter}}; v]$ 
11:    inv $\leftarrow (\nabla \mathbf{F}^h[G_{\text{parameter}}; v])^{-1}$ 
12:     $\delta v \leftarrow \alpha(\text{inv} \cdot \text{res})$ 
13:     $v \leftarrow v - \delta v$ 
14:    if  $|res^\top \delta v|^{1/2} < \text{tol}$  then
15:      break
16:    end if
17:    it $\leftarrow it + 1$ 
18:  end while
19: end for
```

The simulations were implemented in the open-source finite element library Netgen/NGSolve (www.ngsolve.org) [Sch14]. In practice, for those geometries for which the scheme converges successfully, the quantity $|res^\top \delta v|^{1/2}$ became less than the tolerance 10^{-6} after approximately 300 iterations. Hence, each minimization problem involved between 1700 and 1800 Newton iterations.

4.4 Free slip vs. traction-free boundary conditions

For each of the four geometries studied, 100 groups of elements were established at the interface with the substrate. The bonding (the zero-displacement boundary condition) was then removed group of elements by group of elements. So, in all, for each geometry 100 minimization problems were solved (each time a group of elements was detached, the boundary value problem changes).

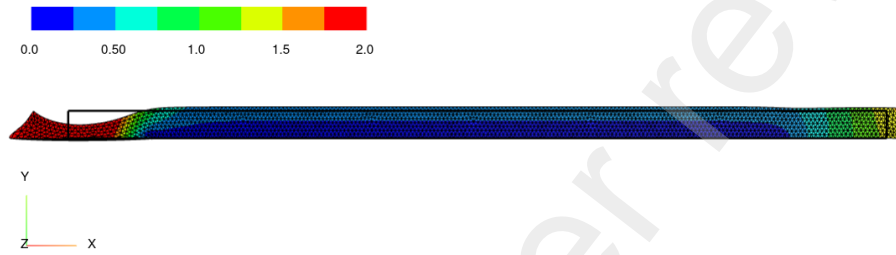


Figure 3: Deformed configuration for $d = 3.00\text{ mm}$ and $\delta = 0.74$ under the traction-free boundary condition in the detached part, after 35 iterations of Newthon's method in the second global cycle. This corresponds to the solution obtained when using the swelling equilibrium of the gel with a shear modulus of 0.91 MPa as the initial approximation for a gel with shear modulus of 0.76 MPa . The rectangle in black shows the reference configuration. The color bar is adjusted to show in red displacements of a magnitude of 2 mm or larger. The code stops running after some more iterations.

The first proposed numerical scheme (20), described above, exhibited a very poor performance:

- In the $90.00\text{ mm} \times 15.00\text{ mm}$ geometry, the code converged only for those meshes with δ between 47% and 77% of bonding (inclusive).
- In the $90.00\text{ mm} \times 3.00\text{ mm}$ geometry, the code converged only for those meshes with δ between 75% and 95% of bonding (inclusive). (Compare Fig. 3 vs. Fig. 4.)
- In the $90.00\text{ mm} \times 1.62\text{ mm}$ geometry, the code converged only for those meshes with δ between 73% and 79% of bonding (inclusive).
- In the $90.00\text{ mm} \times 5.00\text{ mm}$ geometry, the code converged only for those meshes with δ between 74% and 75% of bonding (inclusive).

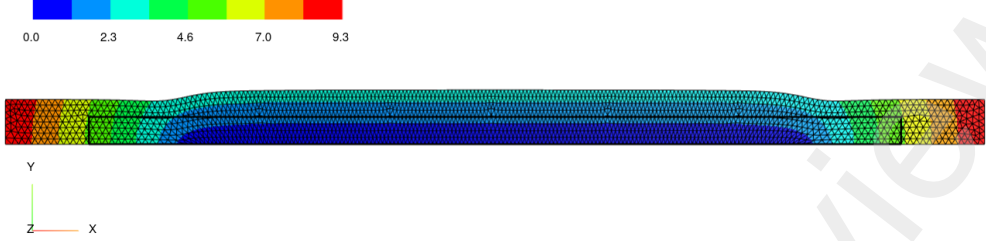


Figure 4: Successful computation of the swelling equilibrium, $d = 3.00\text{ mm}$, $\delta = 0.75$. The color bar is adjusted to show in red the magnitude of the maximum displacement, which is of 9.26 mm . The rectangle in black shows the reference configuration.

Based on our observation that in the successful simulations, during the longitudinal swelling of the detached portion of the gel, its bottom interface remains always essentially at a height $y_2 = 0$, we propose a new numerical scheme consisting in replacing the traction-free boundary condition by a free-slip/zero-vertical-displacement boundary condition on the bottom side of the already detached elements:

$$\text{minimize the total energy } E[u, v] + E_{\text{obstacle}, A}[u, v] \quad \text{in } X_h \times Y_h,$$

where

$$Y_h := \{f \in C(\Omega_2) : f|_T \in \mathcal{P}^3(T), \forall T \in \mathcal{T}_h, f(x_1, 0) = 0, \text{ for all } |x_1| < \frac{\ell}{2}\}.$$

The discrete problem (21) is thus replaced with

$$a(u^h, v^h; \hat{u}^h, \hat{v}^h) = 0 \quad \text{for all } \hat{u}^h \in X_h \text{ and all } \hat{v}^h \in Y_h$$

and the nonlinear system (24)–(25) is changed to the $(m+p) \times (m+p)$ -system

$$F_k^h[u_1, \dots, u_m, v_1, \dots, v_p] = 0 \quad \text{for all } k \in \{1, \dots, m\}$$

and $F_{m+k}^h[u_1, \dots, u_m, v_1, \dots, v_p] = 0 \quad \text{for all } k \in \{1, \dots, p\},$

where, for convenience of notation, we have assumed that (N_1, N_2, \dots, N_p) is precisely the basis of Y_h (note that $Y_h \subset X_h$). The number of degrees of freedom in the implementation in NGSolve for the four geometries studied, both for the traction-free and the free-slip boundary conditions on the debonded part of the interface, are summarized in Table 2.

Table 2: Number of degrees of freedom (respectively, $2m = \dim(X_h)^2$ for the traction-free problem and $m + p = \dim(X_h \times Y_h)$ for the free-slip boundary condition) for a cubic finite element approximation in the two schemes considered.

d [mm]	$\dim(X_h)^2$	$\dim(X_h \times Y_h)$
1.62	16004	15912
3.00	31376	31284
5.00	53204	53112
15.00	159368	159276

This new numerical scheme is much more robust: now the simulations can be carried out in the vast range of δ from 3% bonding all the way up to 85% in the 15.00 mm-thick gel; from 3% to 97% bonding in the geometries with thicknesses of 5.00 mm and 3.00 mm; and from 3% to 100% when $d = 1.62$ mm.

The relative errors committed with this new numerical scheme, compared to the first one, are very small. Different metrics are used to evaluate the quality of the approximation of the new numerical scheme; namely, relative errors are calculated with respect to the:

a) H^1 distance, measured as

$$\frac{\left(\int_{\Omega_2} |u_{\text{FS}} - u_{\text{TF}}|^2 + |v_{\text{FS}} - v_{\text{TF}}|^2 + |\nabla u_{\text{FS}} - \nabla u_{\text{TF}}|^2 + |\nabla v_{\text{FS}} - \nabla v_{\text{TF}}|^2 \right)^{1/2}}{\left(\int_{\Omega_2} |u_{\text{TF}}|^2 + |v_{\text{TF}}|^2 + |\nabla u_{\text{TF}}|^2 + |\nabla v_{\text{TF}}|^2 \right)^{1/2}}$$

where TF and FS in the superscript stand for the traction-free and the free-slip boundary conditions.

- b) Total energy (10).
- c) Deformed length, measured as $y_1(\ell/2, d/2) - y_1(-\ell/2, d/2)$.
- d) Deformed thickness at the middle, measured as $y_2(0, d)$.
- e) Deformed thickness at the far right, measured as $y_2(\ell/2, d)$.
- f) Principal stretches [Gur81] at the middle of the gel and at the right edge of the gel, corresponding to the eigenvalues λ_1 and λ_2 of part \mathbf{U} in the polar decomposition $\mathbf{F} = \mathbf{R}\mathbf{U}$ of the deformation gradient into a rotation \mathbf{R} and a

pure deformation (a symmetric and positive definite tensor) \mathbf{U} . The relative error with respect to these principal stretches is measured here as

$$\frac{\left\| \begin{pmatrix} \lambda_1^{\text{FS}}(0,d) \\ \lambda_2^{\text{FS}}(0,d) \\ \lambda_1^{\text{FS}}(\ell/2,d) \\ \lambda_2^{\text{FS}}(\ell/2,d) \end{pmatrix} - \begin{pmatrix} \lambda_1^{\text{TF}}(0,d) \\ \lambda_2^{\text{TF}}(0,d) \\ \lambda_1^{\text{TF}}(\ell/2,d) \\ \lambda_2^{\text{TF}}(\ell/2,d) \end{pmatrix} \right\|}{\left\| \begin{pmatrix} \lambda_1^{\text{TF}}(0,d) \\ \lambda_2^{\text{TF}}(0,d) \\ \lambda_1^{\text{TF}}(\ell/2,d) \\ \lambda_2^{\text{TF}}(\ell/2,d) \end{pmatrix} \right\|}, \quad (26)$$

where $\|\cdot\|$ denotes the Euclidean norm in \mathbb{R}^4 .

Table 3: The relative errors with respect to the metrics a)-f), expressed as percentages.

d [mm]	δ	a) [%]	b) [%]	c) [%]	d) [%]	e) [%]	f) [%]
1.62	0.73	7.9E-2	3.9E-2	5.6E-4	8.4E-7	1.05	2.9E-5
	0.74	7.8E-2	3.8E-2	5.7E-4	7.3E-7	1.06	2.8E-5
	0.79	7.4E-2	3.7E-2	6.0E-4	3.5E-7	1.05	2.2E-5
3.00	0.77	6.5E-2	3.7E-2	7.5E-4	3.5E-5	4.4E-1	1.6E-4
	0.84	6.1E-2	3.5E-2	4.6E-4	3.1E-5	5.8E-1	1.0E-4
	0.95	4.1E-2	3.5E-2	4.7E-3	1.3E-5	7.5E-1	5.2E-5
5.00	0.74	6.3E-2	3.9E-2	2.6E-4	4.5E-4	3.8E-1	1.4E-3
	0.75	6.3E-2	3.9E-2	2.3E-4	4.3E-4	3.8E-1	1.4E-3
15.00	0.51	6.0E-2	4.8E-2	5.3E-4	2.3E-3	1.5E-1	1.8E-2
	0.60	5.5E-2	4.8E-2	1.2E-3	1.6E-3	1.5E-1	1.3E-2
	0.65	5.2E-2	4.8E-2	1.7E-3	1.5E-3	1.5E-1	1.1E-2

The errors obtained are very small, as can be seen in Table 3. For example, in the four geometries the H^1 distance between the deformations obtained with the two boundary value problems is found to be always below 0.0008 times the H^1 norm of the solution of the original model. Also, the model with the free-slip boundary condition captures the vertical swelling at the middle up to an error of less than 0.0023%. The maximum discrepancy is found in the deformed thickness

$y_2(\ell/2, d)$ at the far right, which nonetheless gives a relative error of less than 1.1%. In all the other metrics the relative errors are under 0.05%.

5 Validation of the thin-film formula for the energy release rate

5.1 Method of approximation of the energy release rate

As mentioned in Section 4.1, four different geometries were studied (90.00 mm long, thicknesses of 1.62, 3.00, 5.00, and 15.00 mm). As mentioned in Section 4.4, 100 minimization problems were solved for each geometry, each corresponding to a different value of δ . Specifically, we worked with the sequence

$$\delta_j := \frac{(100-j)\frac{3}{100} + (j-1)\frac{97}{100}}{99}, \quad j \in \{1, 2, \dots, 100\}$$

of the 100 linearly spaced bonded fractions ranging from 3% to 97%. We approximated the energy-release-rate function $R[\delta]$ defined in (12) first when $\delta = \delta_j$ for some j :

$$R[\delta_j] \approx \frac{\mathcal{E}_{\min}[\delta_j] - \mathcal{E}_{\min}[\delta_{j-1}]}{\ell(\delta_j - \delta_{j-1})}, \quad 2 \leq j \leq 100,$$

then for all $0.0395 \leq \delta \leq 0.97$ by linear interpolation.

We compute, for 100 values of the bonded fraction δ , simulations of the gel deformation, all of these using a single triangulation \mathcal{T}_h , such that each of the corresponding vertices of δ -values is a vertex on the boundary and therefore the edges of the surfaces are either bonded or debonded. This yielded a smooth reconstruction of the energy-release-rate function, as can be observed in Figures 7, 9, 11, and 13.

In the 90.00 mm \times 15.00 mm gel the Newton's method implementation converged only for δ_j with $j \in \{1, \dots, 87\}$ (that is, for $\delta \leq \delta_{87} \approx 84.7\%$). For the other three geometries, the implementation was successful for the 100 meshes. A further sequence of 10 meshes, corresponding to 10 linearly spaced values of δ between 95% and 99.5%, was constructed for the geometries with thicknesses of 1.62 mm and 3.00 mm. In the thin geometry the implementation was successful for all values of δ , whereas for 3.00 mm the computation worked only up to $\delta = 0.97$.

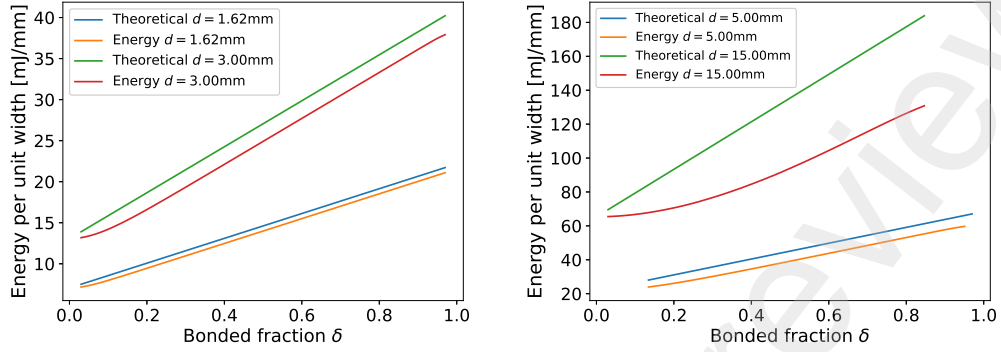


Figure 5: Energies in mJ mm^{-1} , numerical computation and theoretical estimate.

5.2 Energy as a function of δ

The theoretical estimate leading to (14) is

$$\begin{aligned} \mathcal{E}_{\min}[\delta] \approx & \left(d \cdot (\delta \ell) \cdot W_{\text{uni}} + \rho g (\lambda_{\text{uni}} - 1) \frac{d^2}{2} \right) \\ & + \left(d \cdot ((1 - \delta) \ell) \cdot W^* + \rho g (\lambda^* - 1) \frac{d^2}{2} \right), \end{aligned}$$

where W_{uni} and W^* , which are the energy densities related to the optimal stretches λ_{uni} and λ^* defined just above (14), and are given by

$$\begin{aligned} W_{\text{uni}} &:= \frac{G}{2}(1^2 + \lambda_{\text{uni}}^2 + 1^2) + \frac{k_B T}{V_m} H(\lambda_{\text{uni}}) - C, \\ W^* &:= \frac{G}{2}(\lambda^{*2} + \lambda^{*2} + 1) + \frac{k_B T}{V_m} H(\lambda^{*2}), \end{aligned}$$

with C as in (10). Since the gravitational energy density is about four orders of magnitude less than the densities W_{uni} and W^* , then the dependence on δ of this theoretical approximation of the total energy is, essentially, linear. The asymptotic prediction for the energy release rate corresponds to the slope of these affine functions of δ , and is, in particular, proportional to the thickness d .

Figure 5 compare the numerical and the theoretical total energies, as functions of δ , for the four geometries studied. In the 15.00 mm-thick geometry the dependence of the energy on δ is observed to be linear only for the range of values of δ

above 0.4. For the remaining three geometries, the linear dependence is observed in almost the entire range of values of δ , leaving aside only the cases when almost all of the interface Σ has already debonded. In the 15.00 mm gel the smaller slope of the numerical curve compared to the theoretical prediction can easily be noticed, whereas for the other geometries the slope of the real curve is well captured by the asymptotic analysis.

The difference in behaviour between the case when the thickness is 15.00 mm and the thinner gel films is due to the ability of the top part of the gel to swell laterally in spite of the confining force of the bonding substrate, as shall be explained in the coming subsections (see Fig. 12). Something similar occurs for the other geometries in the case when δ is sufficiently small (Figs. 8d and 10d). Note finally that the numerical curves are a small distance below the theoretical approximations: this is because the portion of the gel where the swelling is entirely uniaxial is not the whole of $\{(x_1, x_2, x_3) \in \Omega : |x_1| < \delta\ell\}$, but a shorter region since there is a transition zone where the osmotic tension finds some relief by increasing amounts of lateral swelling (see Figs. 6, 8, and 10).

5.3 1.62 mm thickness

In this geometry the aspect ratio is $1.62/90 \approx 1.8\%$.

Figure 6 shows that for this thin geometry the asymptotic prediction of only two modes of deformation (vertical extension in the middle and equibiaxial expansion on the debonded parts, connected by a small transition region, with a width comparable -by some fixed factor- to the gel thickness) represents well the deformation of the gel.

Figure 7 shows the energy release rate function. The theoretical estimation in (14) is of a release rate that is constant with respect to δ and equal to 168 J m^{-2} . The estimate is correct, up to a 1% error, whenever the fraction δ of the interface that remains bonded is between 17% and 95%; and, up to a 5% error, for δ between 13% and 97%.

5.4 3.00 mm thickness

In this geometry the aspect ratio is $3.00/90 \approx 3.3\%$.

Figure 8 shows that for this thin geometry the asymptotic prediction of only two modes of deformation continues to represent well the deformation of the gel for a large range of values of δ . However, the transition region (between the



$d = 1.62 \text{ mm}, \delta = 0.60.$

Deformed length: 115.64 mm. Average energy density: 0.106 MPa.

$d = 1.62 \text{ mm}, \delta = 0.41.$

Deformed length: 126.81 mm. Average energy density: 0.087 MPa.

$d = 1.62 \text{ mm}, \delta = 0.22.$

Deformed length: 137.97 mm. Average energy density: 0.067 MPa.

Figure 6: Swelling of the $90\text{mm} \times 1.62\text{ mm}$ gel, for three different states of progress of the debonding (60%, 41%, and 21% of bonding, respectively). Colours indicate the energy density $\frac{G}{2}|\mathbf{F}|^2 + \frac{k_B T}{V_m}H(J) - C$ in MPa across the gel. The light blue corresponds to the portions of the gel where the equibiaxial state, with $W(F) = 0.048 \text{ MPa}$, has been attained, whereas the orange portion is where the optimal uniaxial extension, with $W(F) = 0.152 \text{ MPa}$, is attained. The remaining colours indicate the transition from one mode of swelling to the other.

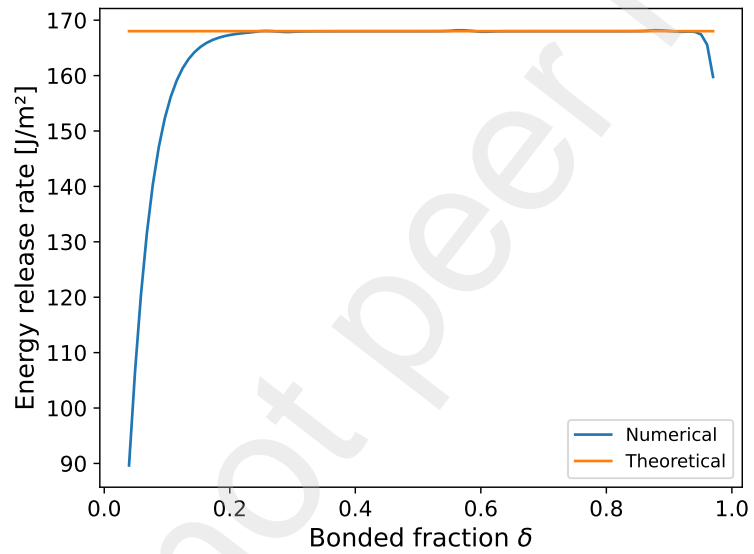


Figure 7: Energy release rate $R[\delta]$ (see Eq. (12)) for the $90\text{ mm} \times 1.62\text{ mm}$ gel, with values in J m^{-2} as a function of the fraction δ of the interface Σ that remains bounded. The theoretical thin-film-limit estimate (14) corresponds to the horizontal bar in orange.



$d = 3.00 \text{ mm}, \delta = 0.94.$

Deformed length: 97.30 mm. Average energy density: 0.138 MPa.

$d = 3.00 \text{ mm}, \delta = 0.51.$

Deformed length: 123.94 mm. Average energy density: 0.093 MPa.

$d = 3.00 \text{ mm}, \delta = 0.27.$

Deformed length: 136.95 mm. Average energy density: 0.068 MPa.

$d = 3.00 \text{ mm}, \delta = 0.08.$

Deformed length: 147.03 mm. Average energy density: 0.051 MPa.

Figure 8: Swelling of the $90 \text{ mm} \times 3.00 \text{ mm}$ gel, for four different states of progress of the debonding (94%, 51%, 27%, and 8% of bonding, respectively). Colours indicate the energy density $\frac{G}{2}|\mathbf{F}|^2 + \frac{k_B T}{V_m}H(J) - C$ in MPa across the gel.

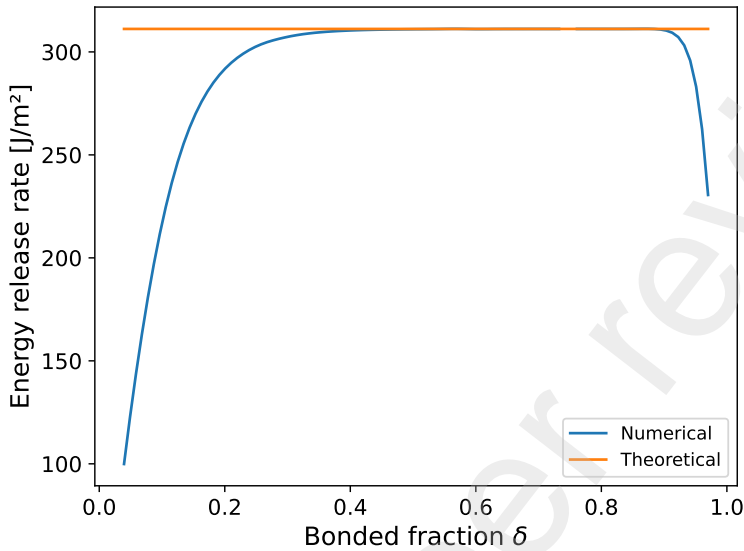


Figure 9: Energy release rate function $R[\delta]$ and thin-film-limit estimate (14) for the $90\text{mm} \times 3.00\text{mm}$ gel.

vertical and the equibiaxial modes of deformation), where the asymptotic energy estimates are no longer accurate, is much wider than in the 1.62 mm-thick gel.

Figure 9 shows the energy release rate function. The theoretical estimation in (14) is of a release rate that is constant with respect to δ and equal to 312 J m^{-2} . The estimate is correct, up to a 1% error, whenever the fraction δ of the interface that remains bonded is between 31% and 91%; and, up to a 5% error, for δ between 22% and 94%.

5.5 5.00 mm thickness

In this geometry the aspect ratio is $5.00/90 \approx 5.6\%$.

Figure 10 shows that for the 5.00 mm-thick geometry the asymptotic vertical and equibiaxial prediction is valid now only for large values of δ , when the portion of the interface that has debonded is still small. For example, when already 45% of the interface has debonded (Fig. 10b), the thin-film description is clearly no longer accurate.

Figure 11 shows the energy release rate function. The theoretical estimation



$d = 5.00 \text{ mm}$, $\delta = 0.80$.

Deformed length: 108.37 mm. Average energy density: 0.118 MPa.



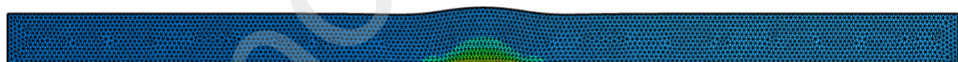
$d = 5.00 \text{ mm}$, $\delta = 0.55$.

Deformed length: 122.85 mm. Average energy density: 0.092 MPa.



$d = 5.00 \text{ mm}$, $\delta = 0.35$.

Deformed length: 134.40 mm. Average energy density: 0.072 MPa.



$d = 5.00 \text{ mm}$, $\delta = 0.13$.

Deformed length: 146.02 mm. Average energy density: 0.053 MPa.

Figure 10: Swelling of the $90 \text{ mm} \times 5.00 \text{ mm}$ gel as the debonding progresses (80%, 55%, 35%, and 13% of bonding, respectively). Colours indicate the energy density $\frac{G}{2}|\mathbf{F}|^2 + \frac{k_B T}{V_m} H(J) - C$ in MPa across the gel.

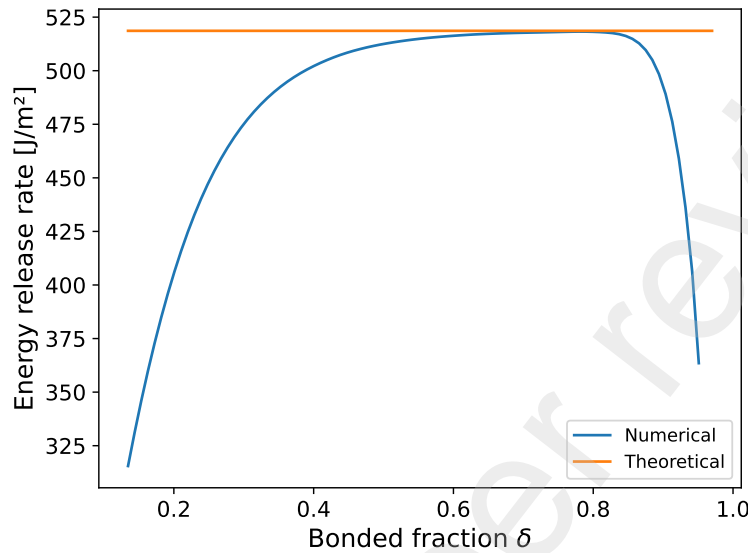


Figure 11: Energy release rate function $R[\delta]$ and thin-film-limit estimate (14) for the 90mm \times 5.00mm gel.

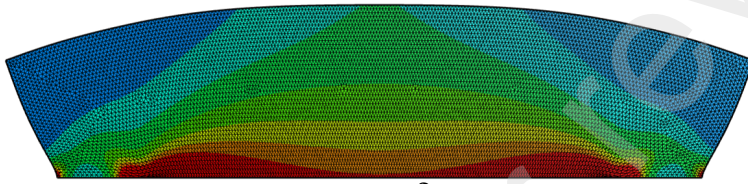
in (14) is of 519 J m^{-2} . Now the range when the estimate is correct up to a 5% error shortens to δ between 35% and 89%, and the range where the error is less than 1% is only for δ from 52% to 86%.

5.6 15.00 mm thickness

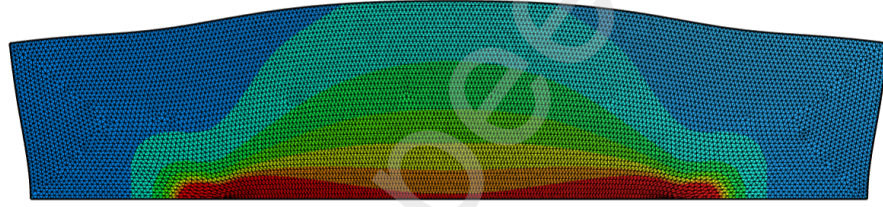
In this geometry the aspect ratio is $15.00/90 \approx 16.7\%$.

Figure 12 shows that the swelling of the 15.00 mm-thick gel is far from the only vertical and equibiaxial thin film limit. This gel has access to a pronounced bending mechanism in which the deformation is the optimal equibiaxial expansion also on the top of the gel, regardless of the efforts of the substrate to restrict the growth of the polymer network only in the vertical direction.

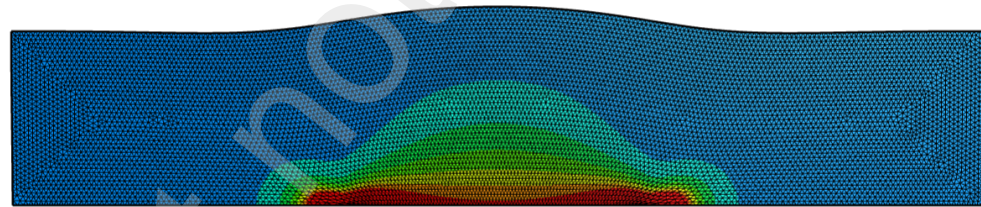
Figure 13 shows the energy release rate function. The theoretical estimation in (14) is of 1556 J m^{-2} . In reality, the maximum release rate is of 1244 J m^{-2} , obtained when 69% of the interface is still bonded. In consequence, the error committed by the thin-film-limit estimation is always greater than 20%. The discrepancy is of less than 30% only when δ is between 50% and 82%.



$d = 15.00 \text{ mm}$, $\delta = 0.85$.
Deformed length: 117.13 mm. Average energy density: 0.097 MPa.



$d = 15.00 \text{ mm}$, $\delta = 0.70$.
Deformed length: 124.83 mm. Average energy density: 0.086 MPa.



$d = 15.00 \text{ mm}$, $\delta = 0.45$.
Deformed length: 137.43 mm. Average energy density: 0.066 MPa.

Figure 12: Swelling of the $90\text{mm} \times 15.00\text{mm}$ gel, for four different states of progress of the debonding (85%, 70%, and 45% of bonding, respectively). Colours indicate the energy density $\frac{G}{2}|\mathbf{F}|^2 + \frac{k_B T}{V_m}H(J) - C$ in MPa across the gel.

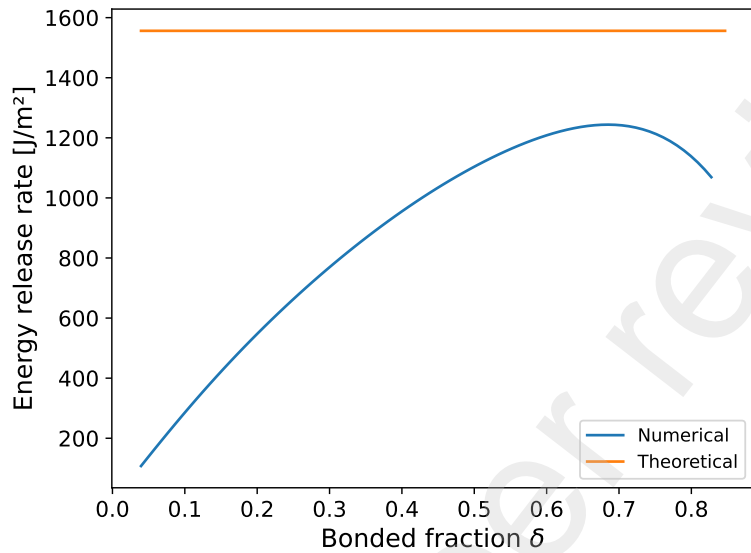


Figure 13: Energy release rate function $R[\delta]$ and thin-film-limit estimate (14) for the $90\text{mm} \times 15.00\text{ mm}$ gel.

Assume that the adhesion toughness σ between the gel and the substrate is around 1100 J m^{-2} , as measured in [YZL⁺16] for swollen hydrogels bonded on glass, and that it remains constant in time. According to Figure 13, a completely bonded $90.0\text{mm} \times 15.00\text{ mm}$ hydrogel, with a shear modulus of $G = 0.13\text{ MPa}$, a Flory-Huggins parameter of $\chi = 0.348$, and an initial polymer volume fraction of $\phi_0 = 0.2$, (in an experiment under $T = 296\text{ K}$ and taking for the molecular volume V_m of the solvent the corresponding value $2.992 \times 10^{-29}\text{ m}^3$ of water,) in a situation of confinement where swelling is possible only upwards and towards the left and or right, would, in principle, be stable against debonding, since its energy release rate $R[\delta]$ is below 1100 J m^{-2} for all $\delta > 0.81$. However, that would involve a risk because if, due to some external driving force, the debonding were initiated and it arrived to the point where, for example, a 23% of the interface is already detached, then, since $R[0.77] = 1188\text{ J m}^{-2}$, the system would become unstable and the gel would spontaneously continue to separate from the substrate. The safer recommendation is that the energy release rate function $R[\delta]$ should be always below the adhesion toughness σ , a criterion that for this gel and for $\sigma = 1100\text{ J m}^{-2}$ does not hold since the maximum release rate, attained at $\delta = 0.68$, is

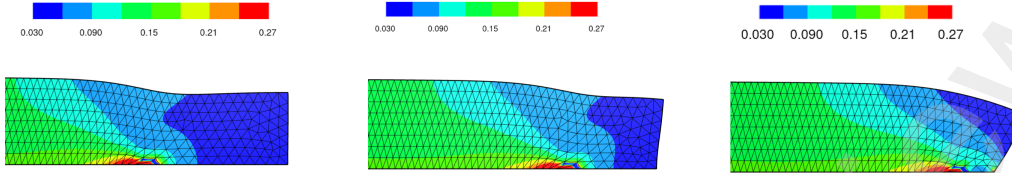


Figure 14: Appearance of a new deformation mode at large values of δ . Thickness: $d = 3.00\text{ mm}$. a) Gel with $\delta = 0.86$, height $y_2(L/2, d)$ after deformation of the upper right corner of the gel: 4.96 mm. b) Gel with $\delta = 0.93$, height of the upper right corner: 4.63 mm. c) Gel with $\delta = 0.97$, height of the upper right corner: 3.80 mm.

of 1244 J m^{-2} .

5.7 Swelling of almost completely bonded gels

Figures 7, 9, and 11 shows a sudden drop of the energy release rate function for large values of delta. Taking as starting point of this descent the value of δ at which the energy release rate departs by more than 1% of the theoretical estimation, for the 1.62 mm-thick gel the descent of the curve begins at $\delta = 0.96$; for the 3.00 mm-thick gel it begins at $\delta = 0.92$; for the 5.00 mm-thick gel it begins at $\delta = 0.87$. The reason is that when only a very small fraction of the interface is debonded, the gel has access to an additional deformation mode leading to an increasingly larger bread-loafing effect, consistent with the measurements and simulations in [SSS⁺22] for the completely bonded gel. This can be appreciated in Figure 14, for the gel with a thickness of 3.00 mm. Note that the right facet remains vertical after swelling whenever $\delta < 0.92$, but that for gels with δ above this value the facet tilts more and more towards the right. Also, the right-end of the gel begins to bend and roll down more and more. That effect can be further verified by the measurements $y_2(L/2, d)$ of the height of the upper right corner of the gel, which decreases from 4.96 mm (the height that is consistently obtained for almost all values of δ) to 3.80 mm when $\delta = 0.97$. If a bending as pronounced as that of Fig. 14c) were to be observed in the situation of the gel of Fig. 14a), clearly a large compression would be induced on an important portion of the gel at the right of the transition region. However, when almost all of the gel is completely bonded, its right-end is allowed to rotate (absorbing more solvent in this way) without inducing any significant compression elsewhere.

6 Conclusions

Incorporating the boundary condition $v(x_1, x_2) = 0$ on $\Sigma \setminus \Gamma$ (the debonded part of the interface) makes the numerical study feasible without introducing any significant errors.

For sufficiently thick gels (such as the 15.00 mm-thickness gel here studied) its swelling is very different from the asymptotic piecewise affine state of only two deformations, one of vertical extension and the other of equibiaxial extension. The reason is that the confining substrate does not prevent the upper part of the gel to swell in the two directions. Even though the difference in deformation between the bottom and the top parts of the gel induces a pronounced bending of the top surface (see Fig. 12), the compression caused by this in the lower corners of the gel is tolerable thanks to the larger thickness of the gel.

Even for thin gels, the simple description of its swelling in terms of the presence of only two deformation modes ceases to be valid when the fraction of the interface that remains bonded becomes very small. Again, in this case the confinement force exerted by the substrate is not transmitted all the way up to the top surface since it can allow itself some bending without causing unsustainable levels of compression in other parts of the gel (see, e.g., Figs. 10d and 8d).

At the other end of the range of possible values of δ something similar happens. The bread-loafing effect observed in [SSS⁺22] for the completely bonded gel (the case $\delta = 1$), with a lateral swelling of the order of 2.00 mm towards the left and right, is also observed in the present study for gels where less than 5% of the interface has debonded (Fig. 14). This provides a tension release mechanism which the gel does not have access to when the fraction $1 - \delta$ of debonded interface is larger. As a consequence, for these large values of δ the energy release rate function drops very rapidly (see especially Figs. 7, 9, and 11) and becomes significantly less than the constant value predicted in the theoretical thin-film limit.

However, for rectangular hydrogels with a thickness-to-length aspect ratio of less than 6%, the description of the swelling as the juxtaposition of the two main deformation modes, with a transition region around the peeling front having a width comparable to the gel's thickness, does capture well the behavior of the system for most values of δ . In particular, the constant value predicted for the energy release rate in the theoretical limit is correct, up to a 5% error, for $\delta \in (0.35, 0.89)$ when $d = 5.00$ mm, for $\delta \in (0.22, 0.94)$ when $d = 3.00$ mm, and for $\delta \in (0.13, 0.97)$ when $d = 1.62$ mm.

Solving the equilibrium equations using the finite element method, for a large number of geometries, each with a different state of progress of the debonding;

and then estimating numerically the energy release rate function; proves to be a successful strategy in order to determine the threshold thickness above which the bonding becomes unstable. The strategy is successful even for thicker gels where the theoretical asymptotic estimate ceases to be valid.

The theoretical estimate (16) for the critical debonding thickness constitutes a lower bound for the real critical thickness. In particular, a flat gel/substrate system with a thickness below the value d_{\max} of (16) is predicted by our study to be safe against debonding. For instance, with the parameters measured in [SSS⁺22], namely: $G = 0.13 \text{ MPa}$, $\chi = 0.348$, $\phi_0 = 0.2$, and $T = 296 \text{ K}$; for a solvent with a molecular volume V_m of $2.992 \times 10^{-29} \text{ m}^3$; and for an adhesion toughness of around 1100 J m^{-2} , as measured in [YZL⁺16] for swollen hydrogels bonded on glass, assuming that it remains constant in time; the estimate for the critical d_{\max} is of 10.60 mm . Therefore, any flat hydrogel with a thickness of less than 10.60 mm , confined by walls on the back and on the front so that the deformation is two-dimensional, will be stable against debonding. The three-dimensional case, in which a lateral swelling is allowed also along the width direction, will be investigated in a subsequent work.

Acknowledgements

S.S. & M.C.C. were funded by National Science Foundation grant DMS-1616866. M.S. was supported by FONDECYT Regular grant N. 1221189 and by Centro Nacional de Inteligencia Artificial CENIA, FB210017, Basal ANID Chile. D.H. was funded by FONDECYT 1190018.

References

- [Bal77] J. M. Ball. Convexity conditions and existence theorems in nonlinear elasticity. *Arch. Ration. Mech. Anal.*, 63:337–403, 1977.
- [Bal81] J M Ball. Global invertibility of Sobolev functions and the interpenetration of matter. *Proc. Roy. Soc. Edinb. Sect. A*, 88(3-4):315–328, 1981.
- [BCO81] J M Ball, J C Currie, and P J Olver. Null Lagrangians, weak continuity, and variational problems of arbitrary order. *J. Funct. Anal.*, 41(2):135–174, 1981.

- [BFM08] Blaise Bourdin, Gilles A Francfort, and Jean-Jacques Marigo. The variational approach to fracture. *J. Elasticity*, 91(1-3):5–148, 2008.
- [BHMCR23a] Marco Barchiesi, Duvan Henao, Carlos Mora-Corral, and Rémy Rodiac. Harmonic dipoles and the relaxation of the neo-Hookean energy in 3D elasticity. *arXiv:2102.12303*, 2023.
- [BHMCR23b] Marco Barchiesi, Duvan Henao, Carlos Mora-Corral, and Rémy Rodiac. On the lack of compactness problem in the axisymmetric neo-Hookean model. *arXiv:2111.07112*, 2023.
- [Bra02] Andrea Braides. *Γ -convergence for beginners*, volume 22 of *Oxford Lecture Series in Mathematics and its Applications*. Oxford University Press, Oxford, 2002.
- [CDL03] S. Conti and C. De Lellis. Some remarks on the theory of elasticity for compressible Neohookean materials. *Ann. Sc. Norm. Super. Pisa Cl. Sci. (5)*, 2(3):521–549, 2003.
- [CGH⁺20] M. C. Calderer, C. Garavito, D. Henao, S. Lyu, and L. Tapia. Gel debonding from a rigid substrate. *J. Elast.*, 141:51–73, 2020.
- [CH23] M. C. Calderer and D. Henao. Asymptotic analysis of an internal transition layer in a planar gel debonding problem. *Submitted*, 2023.
- [Cia78] Philippe G. Ciarlet. *The finite element method for elliptic problems*. Number 4 in Studies in Mathematics and its Applications. North-Holland Publishing Co., 1978.
- [Cia88] Philippe G. Ciarlet. *Mathematical elasticity. Vol. I*, volume 20 of *Studies in Mathematics and its Applications*. North-Holland Publishing Co., Amsterdam, 1988.
- [CN87] Philippe G. Ciarlet and Jindřich Nečas. Injectivity and self-contact in nonlinear elasticity. *Arch. Rational Mech. Anal.*, 87:171–188, 1987.
- [Dac08a] Bernard Dacorogna. *Direct methods in the calculus of variations*, volume 78 of *Applied Mathematical Sciences*. Springer, New York, second edition, 2008.

- [Dac08b] Bernard Dacorogna. *Introduction To The Calculus Of Variations*. Imperial College Press, second edition, 2008.
- [Dal93] Gianni Dal Maso. *Introduction to Γ -Convergence*. Birkhäuser, 1993.
- [DHM23] Anna Doležalová, Stanislav Hencl, and Jan Malý. Weak limit of homeomorphisms in $W^{1,n-1}$ and (INV) condition. *arXiv:2112.08401*, 2023.
- [Doi13] Masao Doi. *Soft matter physics*. Oxford University Press, 2013.
- [EG92] L C Evans and R F Gariepy. *Measure theory and fine properties of functions*. CRC Press, Boca Raton, FL, 1992.
- [Eva10] Lawrence C Evans. *Partial differential equations*, volume 19 of *Graduate Studies in Mathematics*. American Mathematical Society, Providence, RI, second edition, 2010.
- [Flo41] P J Flory. Molecular size distribution in three dimensional polymers. I. Gelation. *J. Amer. Chem. Soc.*, 63:3083–3090, 1941.
- [Flo53] P.J. Flory. *Principles of Polymer Chemistry*. Cornell U. Press, 1953.
- [FM98] G.A. Francfort and J.-J. Marigo. Revisiting brittle fracture as an energy minimization problem. *Journal of the Mechanics and Physics of Solids*, 46(8):1319 – 1342, 1998.
- [FRJ43] Paul J Flory and John Rehner Jr. Statistical mechanics of cross-linked polymer networks i. rubberlike elasticity. *The journal of chemical physics*, 11(11):512–520, 1943.
- [FRJ44] Paul J Flory and John Rehner Jr. Effect of deformation on the swelling capacity of rubber. *The Journal of Chemical Physics*, 12(10):412–414, 1944.
- [GMS89] Mariano Giaquinta, Giuseppe Modica, and Jiří Souček. Cartesian currents, weak diffeomorphisms and existence theorems in nonlinear elasticity. *Arch. Rational Mech. Anal.*, 106(2):97–159, 1989.

- [Gri21] Alan A. Griffith. VI. The phenomena of rupture and flow in solids. *Philosophical transactions of the royal society of london. Series A, containing papers of a mathematical or physical character*, 221(582-593):163–198, 1921.
- [Gur81] M. E. Gurtin. *An introduction to Continuum Mechanics*. Number 158 in Mathematics in Science and Engineering. Academic Press, 1981.
- [HH14] Daniel Hurtado and Duvan Henao. Gradient flows and variational principles for cardiac electrophysiology: Toward efficient and robust numerical simulations of the electrical activity of the heart. *Comput. Methods Appl. Mech. Engrg.*, 273:238–254, 2014.
- [HMC10] Duvan Henao and Carlos Mora-Corral. Invertibility and weak continuity of the determinant for the modelling of cavitation and fracture in nonlinear elasticity. *Archive for Rational Mechanics and Analysis*, 197(2):619–655, 2010.
- [HMCX16] Duvan Henao, Carlos Mora-Corral, and Xianmin Xu. A numerical study of void coalescence and fracture in nonlinear elasticity. *Comput. Methods Appl. Mech. Engrg.*, 303:163–184, 2016.
- [HR18] Duvan Henao and Rémy Rodiac. On the Existence of minimizers for the Neo-hookean energy in the axisymmetric setting. *Disc. Cont. Dyn. Sys.*, 38(9):4509–4536, 2018.
- [Hug41] M L Huggins. Solutions of long chain compounds. *J. Chem. Phys.*, 9:440, 1941.
- [M90] Stefan Müller. Higher integrability of determinants and weak convergence in L^1 . *J. Reine Angew. Math.*, 412:20–34, 1990.
- [MS95] Stefan Müller and Scott J. Spector. An existence theory for nonlinear elasticity that allows for cavitation. *Archive for Rational Mechanics and Analysis*, 131(1):1–66, 1995.
- [MTY94] S. Müller, Q. Tang, and B.S. Yan. On a new class of elastic deformations not allowing for cavitation. *Ann. Inst. H. Poincaré Anal. Non Linéaire*, 11:217–243, 1994.

- [Muc10] Domenico Mucci. A variational problem involving the distributional determinant. *Riv. Mat. Univ. Parma (N.S.)*, 1(2):321–345, 2010.
- [Mül88] Stefan Müller. Weak continuity of determinants and nonlinear elasticity. *C. R. Acad. Sci. Paris Sér. I Math.*, 307(9):501–506, 1988.
- [RC⁺03] Michael Rubinstein, Ralph H Colby, et al. *Polymer physics*, volume 23. Oxford university press New York, 2003.
- [Sch14] J. Schöberl. C++11 implementation of finite elements in NG-Solve. Technical Report 30, Vienna University of Technology - Institute for Analysis and Scientific Computing, 2014.
- [SSS⁺22] Sichen Song, Ronald A. Siegel, Manuel A. Sánchez, M. Carme Calderer, and Duvan Henao. Experiments, modelling, and simulations for a gel bonded to a rigid substrate. *J. Elast.*, 2022.
- [Šve88] V Šverák. Regularity properties of deformations with finite energy. *Arch. Rational Mech. Anal.*, 100(2):105–127, 1988.
- [YZL⁺16] Hyunwoo Yuk, Teng Zhang, Shaoting Lin, German Alberto Parada, and Xuanhe Zhao. Tough bonding of hydrogels to diverse non-porous surfaces. *Nature Materials*, 15:190–196, 2016.